J Mater Sci (2008) 43:852–859
DOI 10.1007/s10853-007-2179-4

Sintering kinetics at constant rates of heating: effect of GeO_2 addition on the initial sintering stage of 3 mol% Y_2O_3-doped zirconia powder

Koji Matsui · Junichi Hojo

Received: 7 February 2007 / Accepted: 20 September 2007 / Published online: 31 October 2007

Abstract The sintering behavior of 3 mol% Y_2O_3-doped zirconia powders with and without a small amount of GeO_2 was investigated to clarify the effect of GeO_2 addition on the initial sintering stage. The shrinkage of powder compact was measured under constant rates of heating (CRH). The sintering rate was accelerated by GeO_2 addition, and increased with increasing GeO_2 content. The mechanism, apparent activation energy (nQ), and apparent frequency factor (β_0^n) of diffusion at the initial sintering stage were estimated using the sintering-rate equations that are applicable to the CRH data. The sintering mechanism changed from grain-boundary (GBD) to volume diffusions (VD) by GeO_2 addition, and both nQ and β_0^n of diffusion increased with increasing GeO_2 content. It is, therefore, concluded that the enhanced sintering mechanism by GeO_2 addition is explained by the GBD→VD change and increases in both nQ and β_0^n of diffusion at the initial sintering stage.

Introduction

Yttria-stabilized tetragonal zirconia polycrystal (Y-TZP) has been known as an important structural ceramic with excellent mechanical properties such as high strength and fracture toughness, and is used for products of the optical fiber connector, grinding media, and precision parts. The hydrolysis process is known as the industrial manufacturing process for raw powder of these Y-TZP ceramics. The appearance of Y-TZP with both higher characteristic and reliability is desired to spread the zirconia-product market. It is thought that such a Y-TZP is created from the raw material powder which is sintered at a lower temperature.

So far, the initial stage of sintering on various ceramic powders has been investigated by many researchers [1–12]. Young and Cutler [1] have investigated the initial sintering behavior in yttria-stabilized zirconia under constant rates of heating (CRH). Wang and Raj [2, 3] have estimated the activation energies at the intermediate sintering stage of zirconia (with Y_2O_3), and Al_2O_3/zirconia (with Y_2O_3) composite by the CRH method. In previous papers, Matsui and Hojo have analyzed both initial sintering behaviors in Y-TZP and yttria-stabilized cubic stabilized zirconia (Y-CSZ) powders with a small amount of Al_2O_3 using the CRH technique, and reported that with both powders, Al_2O_3 changes the sintering mechanism from grain-boundary (GBD) to volume diffusions (VD) at the initial sintering stage and remarkably enhanced the densification rate because of a decrease in the activation energy [4, 5].

From the standpoint of a new product development, it is especially important to clarify the action mechanisms of various additives that accelerate the sintering rate in Y-TZP. Al_2O_3 is usually used as one of the additives, and the sintering-acceleration actions of Al_2O_3 have been clarified as described above [4, 5]. Recently, GeO_2 is noted as the doping agent that accelerates the high temperature plastic flow in Y-TZP, and the superplasticity behavior and microstructure in GeO_2-doped Y-TZP has been investigated [13–16]. For the microstructure development during sintering, Yoshida et al. [13] have reported that the grain-growth rate in Y-TZP was enhanced by GeO_2-dopoing. It is

K. Matsui (✉)
Tokyo Research Laboratory, Tosoh Corporation, 2743-1, Hayakawa, Ayase, Kanagawa 252-1123, Japan
e-mail: k_matui@tosoh.co.jp

J. Hojo
Department of Applied Chemistry, Faculty of Engineering, Kyushu University, Fukuoka 819-0395, Japan

thought from their result that GeO_2 influences not only grain-growth but also densification processes in Y-TZP during sintering. However, the effect of GeO_2 addition on the densification process has not been reported in previous papers [13–16].

In the present study, GeO_2, which is one of the additives, was noted, and the effect of GeO_2 addition on initial sintering of Y-TZP powder produced by the hydrolysis process was investigated.

Experimental procedure

Specimen preparation

The Y-TZP powder containing 3 mol% (5.2 mass%) Y_2O_3 with a specific surface area of 15 m^2/g (3Y000G; TZ-3Y grade, Tosoh, Tokyo, Japan) and the GeO_2 powder (purity >99.99%, cica-reagent, Kanto Chemical, Tokyo, Japan) were used as starting materials. Y-TZP powders with 0.25, 0.5, and 0.77 mass% GeO_2 was prepared by wet-milling the Y-TZP and GeO_2 powders with a vibration mill. These powders are termed 3Y025G, 3Y050G, and 3Y077G, respectively. The prepared powders were pressed uniaxially into a disk under 70 MPa. The resulting powder compacts were sintered at 1,300 and 1,500 °C for 2 h in air (heating rate 100 °C/h).

Density and grain-size measurements

The density of sintered bodies was measured using the Archimedes method. However, in case of the sintered bodies with relative densities of <80%, the density was calculated from the weight and size. Scanning electron microscopy (SEM; Model S-4500, Hitachi, Tokyo, Japan) was used to measure the average grain sizes of the sintered bodies. SEM specimens were polished with a 3-μm diamond paste, and then thermally etched for 1 h at a temperature that was 50 °C lower than the sintering temperature of each specimen in air. The average grain size was measured by the Planimetric method [17].

CRH measurements

The prepared powders were pressed uniaxially into a columnar disk under ~100 MPa and then pressed isostatically at 200 MPa by rubber pressing. The resulting powder compacts were of the size 6 mm ∅ × 15 mm. The shrinkage of the powder compacts with sintering was measured using a dilatometer (Model DL 9700, ULVAC-RIKO, Yokohama, Japan). In a dilatometer, the shrinkage proceeds isotropically because only a slight load was hung to the specimen during the measurement. The shrinkage measurements by CRH techniques were performed in the range from room temperature to 1,500 °C at heating rates of 5, 10, 15, and 20 °C/min in air. When the temperature reached 1,500 °C, the specimens were cooled at a constant rate. The dilatometer was calibrated using sapphire as a standard specimen. Thermal expansion of each specimen was corrected by the same method in the previous paper [4]. Assuming isotropic shrinkage to powder compact, the density $\rho(T)$ at a given temperature (T) is given by the following equation [2]:

$$\rho(T) = \left(\frac{L_f}{L(T)}\right)^3 \rho_f \tag{1}$$

where L_f and $L(T)$ are the final length and the length at a T of the specimen, respectively. ρ_f indicates the final density measured by the Archimedes method. The $\rho(T)$ value at a T was calculated using Eq. 1.

CRH-data analysis

The material-transport path and activation energy of diffusion at the initial sintering stage were determined by the same analytical method as that in the previous paper [5]. The sintering-rate equation at the initial sintering stage is given by the following equation [7]:

$$\frac{d}{dt}\left[\left(\frac{\Delta L}{L_0}\right)^{1/n}\right] = \frac{K\gamma\Omega D}{kTa^p} \tag{2}$$

where $\Delta L(=L_0 - L)$ is the change in length of the specimen, L_0 the initial length of the specimen, K the numerical constant, γ the surface energy, Ω the atomic volume, D the diffusion coefficient, t the time, T absolute temperature, k the Boltzmann's constant, a the particle radius, and the parameters n and p the order depending on the diffusion mechanism. The values of p for GBD and VD are $p = 4$ and $p = 3$, respectively. Equation 2 is applicable to the fractional shrinkages of <4% that satisfy the initial sintering condition.

The following sintering-rate equation that is applicable to CRH data is derived from Eq. 2 [5].

$$\ln\left[T\left(\frac{dT}{dt}\right)\left(\frac{d\rho}{dT}\right)\right] = -\frac{Q}{RT} + \alpha_{1/n} \tag{3}$$

where

$$\alpha_{1/n} = \ln\left[f_{1/n}(\rho)\right] + \ln\left[\frac{K\gamma\Omega D_0}{k}\right] - p\ln a \tag{4}$$

Here, Q is the activation energy, R the gas constant, $f_{1/n}(\rho)$ the density function, and D_0 the pre-exponential

term defined as $D = D_0 \exp(-Q/RT)$. Equation 3 corresponds to the sintering-rate equation derived by Wang and Raj [2]. Using the slope S_1 of the Arrhenius-type plot of $\ln[T(dT/dt)(d\rho/dT)]$ against $1/T$ at the same density, the activation energy is expressed as

$$Q = -RS_1 \tag{5}$$

On the other hand, the following sintering-rate equation that is different from Eq. 3 is also derived from Eq. 2 [5].

$$\frac{d(\Delta L/L_0)}{dT} = \left(\frac{K\gamma\Omega D_0 R}{ka^p cQ}\right)^n \left(\frac{nQ}{RT^{2-n}}\right) \exp\left(-\frac{nQ}{RT}\right) \tag{6}$$

Here, c is the heating rate. For $n = 1/3$ and $n = 1/2$, this rate equation corresponds to the sintering-equations derived by Young and Cutler [1]. This rate equation is also applied to CRH data. Using the slope S_2 of the Arrhenius-type plot of $\ln[T^{2-n}d(\Delta L/L_0)/dT)]$ against $1/T$, the apparent activation energy nQ is expressed as

$$nQ = -RS_2 \tag{7}$$

Here, n is in the range of 0.31–0.50 [6]. In the previous paper, Matsui and Hojo have reported that the values of nQ in 3 mol% (5.3 mass%) Y-TZP powder with a specific surface area of 6.7 m^2/g determined from Arrhenius-type plots that correspond to $n = 1/3$ and $n = 1/2$ were 219 and 217 kJ/mol, respectively [4]. This result suggests that nQ is almost the same value in the range of $n = 0.31$–0.50. Therefore, S_2 may be estimated as the approximate value from the Arrhenius-type plot of $\ln[T^{1.6}d(\Delta L/L_0)/dT)]$ against $1/T$ that corresponds to $n = 0.4$, which is the central value of $n = 0.31$–0.50 [5]. Combining Eqs. 5 and 7, the following equation is obtained [5]:

$$n = \frac{nQ}{Q} = \frac{S_2}{S_1} \tag{8}$$

In the present analysis, both Q and n were determined at the fractional shrinkages of <4% that satisfy the initial sintering condition.

Results and discussion

Densification and grain growth

Figure 1 shows the change of relative densities of 3Y000G, 3Y025G, 3Y050G, and 3Y077G (3Y000G–3Y077G) with sintering temperature. The relative density of 3Y025G (with 0.25 mass% GeO_2) was higher than that of 3Y000G (without GeO_2) at lower temperatures, and attained 99% at 1,350 °C. When the GeO_2 content increased further, the relative density became high at lower temperature. At the

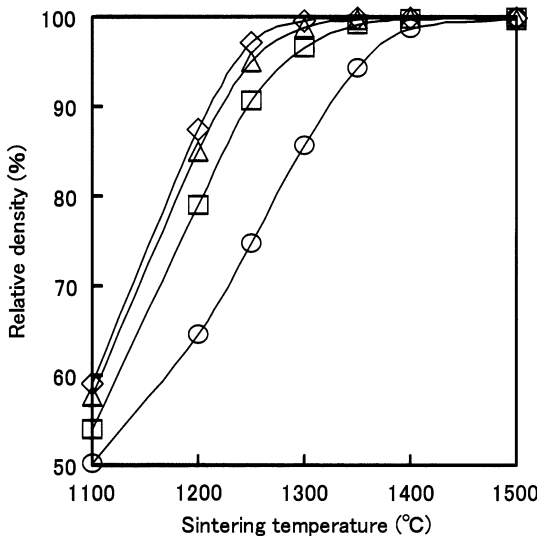

Fig. 1 Changes of relative densities in 3Y000G, 3Y025G, 3Y050G, and 3Y077G with sintering temperature. The duration time at each sintering temperature is 2 h. (○), (□), (Δ), and (◇) indicate 3Y000G, 3Y025G, 3Y050G, and 3Y077G, respectively

GeO_2 content of 0.77 mass%, the relative density attained 99% at 1,300 °C. This result reveals that the densification rate is remarkably accelerated by GeO_2 addition, and increases with increasing GeO_2 content.

Figure 2 shows SEM images of the polished and etched surface of 3Y000G–3Y077G sintered at 1,500 °C. The grain size changed little in the GeO_2-content range of 0–0.77 mass%. To quantitatively examine the effect of GeO_2 addition on grain growth, the average grain sizes of 3Y000G–3Y077G sintered at 1,300 and 1,500 °C were determined by the Planimetric method. As shown in Fig. 3, the average grain sizes of 3Y000G–3Y077G sintered at each temperature were nearly of the same value. This result suggests that at the hold time of 2 h in the present sintering profiles, the effect of GeO_2 content does not clearly appear for the grain-growth process.

Densification behavior by CRH

The shrinkage behavior of the powder compacts of 3Y000G–3Y077G was measured to examine the effect of GeO_2 addition on the sintering rate. Figure 4 shows the changes of the shrinkage of 3Y000G–3Y077G with temperature in the course of 5 °C/min heating. As can be seen in Fig. 4a, the starting sintering temperatures of 3Y000G–3Y077G are almost the same, and the shrinkages of 3Y025G, 3Y050G, and 3Y077G were clearly greater than that of 3Y000G at temperatures of $\geq\sim$1,050 °C. The shrinkage rate increased with increasing GeO_2 content, and showed nearly the same behavior at GeO_2 contents of

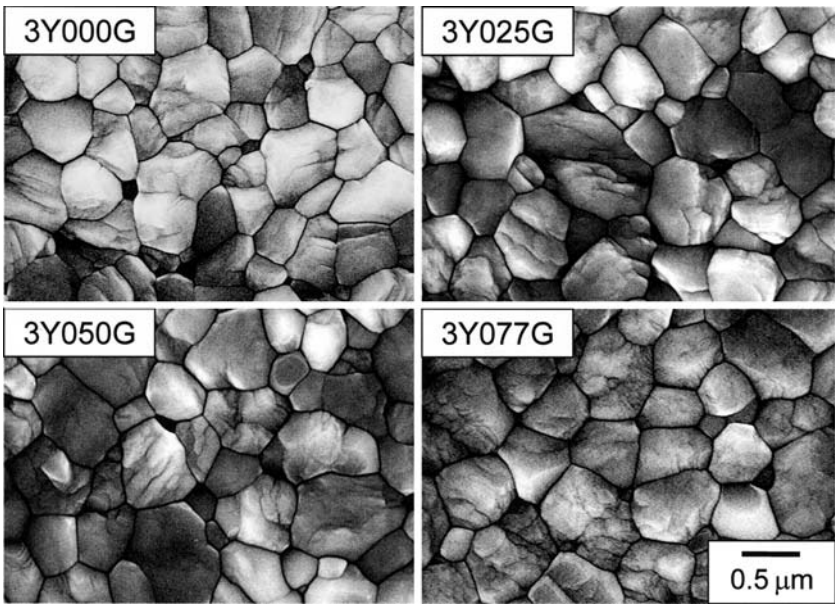

Fig. 2 Scanning electron microscopy images of 3Y000G, 3Y025G, 3Y050G, and 3Y077G sintered at 1,500 °C

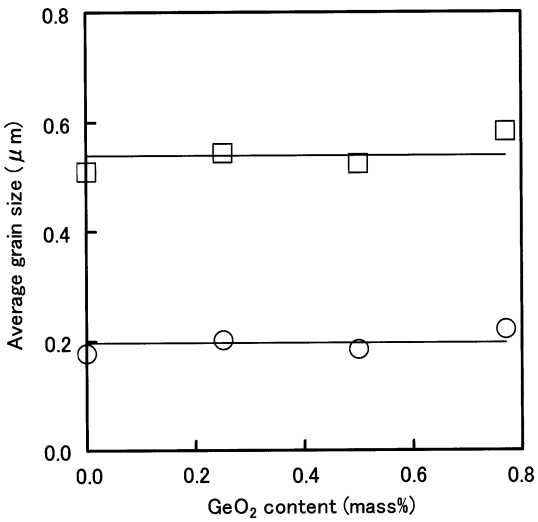

Fig. 3 GeO_2-content dependence of average grain sizes in Y-TZP sintered at 1,300 and 1,500 °C for 2 h. (○) and (□) indicate 1,300 and 1,500°C, respectively

≥0.5 mass%. Using each shrinkage curve in Fig. 4a, the temperature dependence of the relative density was determined by Eq. 1 (Fig. 4b). The relative densities of 3Y025G, 3Y050G, and 3Y077G were clearly higher than that of 3Y000G at temperatures of ≥∼1,050 °C. These results indicate that the sintering rate increases with increasing GeO_2 content, and the behavior is nearly the same at GeO_2 contents of ≥0.5 mass%.

Figure 5 shows the temperature dependence of the densification rates ($d\rho/dT$) of (a) 3Y000G and (b) 3Y025G measured at 5–20 °C/min heating rates. The densification-rate curves of both 3Y000G and 3Y025G shifted to a higher temperature, as the heating rate increased. The shift of the densification-rate curve of 3Y025G with the increase in heating rate was greater than that of 3Y000G.

Analysis of initial sintering mechanism

To quantitatively investigate the effect of GeO_2 addition on the sintering rate, the activation energies of diffusion at the initial sintering stage in 3Y000G and 3Y025G were determined by applying Eq. 3 to the results in Figs. 4 and 5. Equation 3 can be applied in the following way. For different dT/dt values of 5, 10, 15, and 20 °C/min, the T and $d\rho/dT$ values at the same relative density were determined, respectively, and their values were plotted as the Arrhenius-type plot of $T(dT/dt)(d\rho/dT)$ against $1/T$ (Fig. 6). The values of activation energy and $\alpha_{1/n}$ at each relative density were determined from the slope and intercept of the straight line in the Arrhenius-type plot, respectively. Here, this analysis was performed in the relative-density range of ≤54% that corresponds to the fractional shrinkages of <4%. Figure 7 shows the activation energy and $\alpha_{1/n}$ of 3Y000G and 3Y025G at 50–54% densities. At each density, both values of activation energy and $\alpha_{1/n}$ of 3Y025G were lower than those of 3Y000G. The average values (Q) of activation energy in 3Y000G and 3Y025G were calculated using the numerical values in Fig. 7a. As shown in Table 1, it is seen that the Q value of 3Y025G is smaller than that of 3Y000G. The Q value of 3Y000G agreed nearly with that of 3 mol% Y-TZP powder in the previous paper [4]. The present results reveal that the activation energy of diffusion at the initial sintering stage decreases by GeO_2 addition.

It is speculated that this decrease in the Q value occurs by the change of the diffusion mechanism. To estimate the

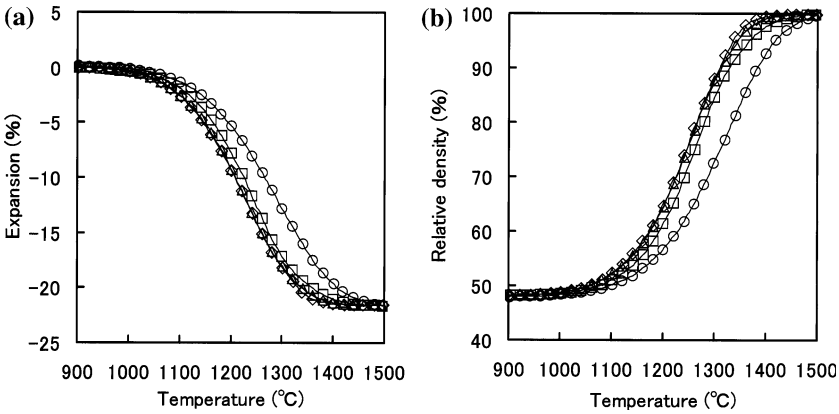

Fig. 4 Temperature dependence of (**a**) shrinkage and (**b**) relative density of 3Y000G, 3Y025G, 3Y050G, and 3Y077G in the course of heating (5 °C/min). (○), (□), (Δ), and (◇) indicate 3Y000G, 3Y025G, 3Y050G, and 3Y077G, respectively

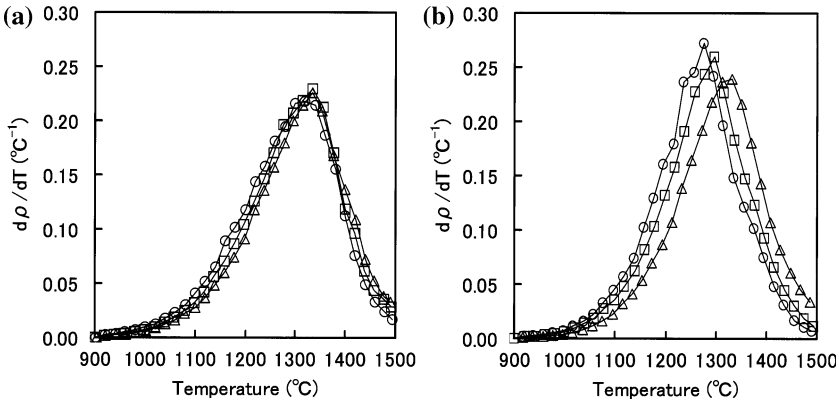

Fig. 5 Temperature dependence of densification rate of (**a**) 3Y000G and (**b**) 3Y025G at various heating rates. (○), (□), and (Δ) indicate 5, 10, and 20 °C/min, respectively. The data measured at a 15 °C/min heating rate were also obtained in a similar manner

order depending on the diffusion mechanism, the apparent activation energies of 3Y000G and 3Y025G were determined by applying Eq. 6 to the results in Fig. 4a. Equation 6 can be applied in the following way. In the same fractional shrinkage range as above, the nQ values were determined from the slopes of the Arrhenius-type plot of $\ln[T^{1.6}\mathrm{d}(\Delta L/L_0)/\mathrm{d}T)]$ against $1/T$. As an example, the plots of $\ln[T^{1.6}\mathrm{d}(\Delta L/L_0)/\mathrm{d}T)]$ against $1/T$ for 3Y000G and 3Y025G at a 5 °C/min heating rate are shown in Fig. 8. Both plots of 3Y000G and 3Y025G revealed linear relations, in which the slope of 3Y025G was grater than that of 3Y000G. The apparent activation energies were estimated as the mean of the nQ values that were determined from the Arrhenius-type plots of $\ln[T^{1.6}\mathrm{d}(\Delta L/L_0)/\mathrm{d}T)]$ against $1/T$ at 5–20 °C/min heating rates, respectively (Table 1). The nQ value of 3Y025G was greater than that of 3Y000G.

Using the Q and nQ values in Table 1, the orders (n) depending on the diffusion mechanism at the initial sintering stage were determined by Eq. 8 (Table 1). The n values of 3Y000G and 3Y025G were 0.32 and 0.45, respectively. According to two-sphere shrinkage models proposed by several researchers, the n value ranges of GBD and VD are 0.31–0.33 and 0.40–0.50, respectively [6]. Comparing them with the above n values determined experimentally, the diffusion mechanisms of 3Y000G and 3Y025G are assigned to GBD and VD, respectively. The

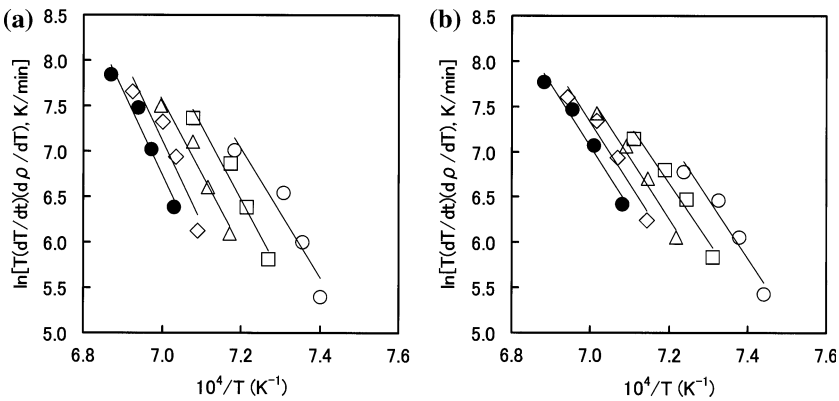

Fig. 6 Arrhenius-type plots of (**a**) 3Y000G and (**b**) 3Y025G for the estimate of activation energies of sintering. (○), (□), (Δ), (◇), and (●) represent 50, 51, 52, 53, and 54% relative densities, respectively. The data of 50.5, 51.5, 52.5, and 53.5% relative densities were also obtained in a similar manner

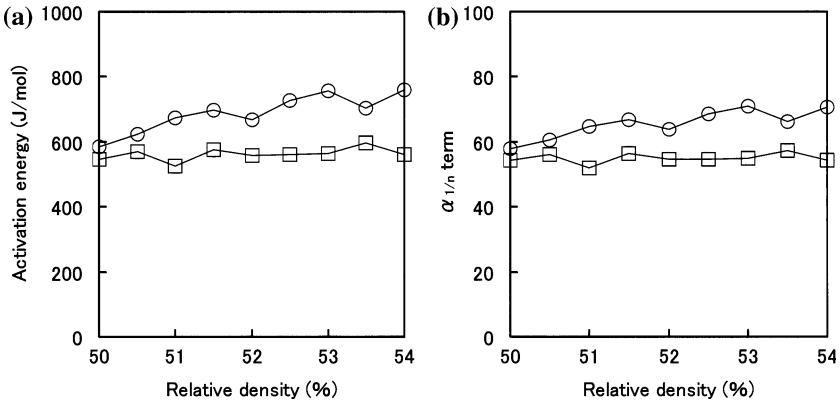

Fig. 7 Activation energy and $\alpha_{1/n}$ of 3Y000G and 3Y025G at 50–54% relative densities. (○) and (□) indicate 3Y000G and 3YC025G, respectively

Table 1 Activation energies, apparent activation energies, and orders depending on diffusion mechanism at initial sintering stage

Specimen	Activation energy (kJ/mol)		Apparent activation energy (kJ/mol)		Order on diffusion mechanism
	Q	Standard deviation	nQ	Standard deviation	n
3Y000G	688	58	222	5	0.32
3Y025G	561	20	253	5	0.45

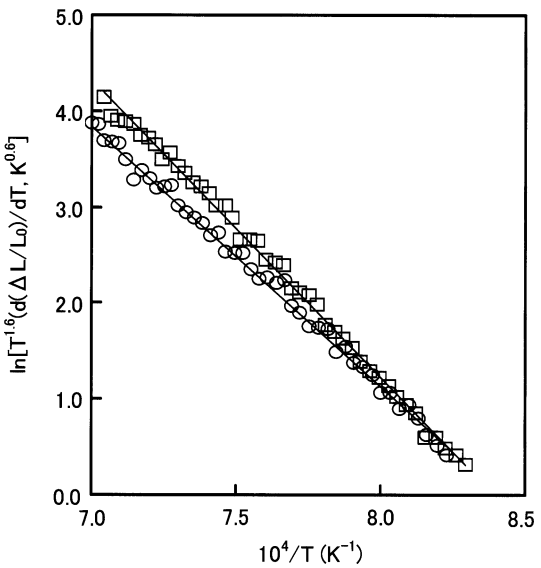

Fig. 8 Plots of $\ln[T^{1.6}\mathrm{d}(\Delta L/L_0)/\mathrm{d}T)]$ against $1/T$ of 3Y000G and 3Y025G in the course of heating (5 °C/min). (○) and (□) indicate 3Y000G and 3Y025G, respectively

diffusion mechanism (i.e., GBD) of 3Y000G agreed with that of 3 mol% Y-TZP in the previous paper [4]. This result reveals that the diffusion mechanism changes from GBD to VD by GeO_2 addition.

According to the results in Figs. 1 and 4, the sintering rate increases with increasing GeO_2 content. To clarify the effect of CeO_2 content on the sintering rate, the activation energy and frequency-factor term (that is defined by the following β_0) of each specimen are estimated using Eq. 6. Putting as $\beta_0 = (K\gamma\Omega D_0)/(ka^p)$, Eq. 6 is expressed by

$$\frac{\mathrm{d}(\Delta L/L_0)}{\mathrm{d}T} = \beta_0^n \left(\frac{R}{cQ}\right)^n \left(\frac{nQ}{RT^{2-n}}\right) \exp\left(-\frac{nQ}{RT}\right) \tag{9}$$

For GeO_2 and no GeO_2 additions, the n values are 0.45 and 0.32, respectively. Using Eq. 9, in which these n values are substituted, and the shrinkage curves in Fig. 4a, the Q values were determined from the slopes of the Arrhenius-type plots of $\ln[T^{1.68}\mathrm{d}(\Delta L/L_0)/\mathrm{d}T)]$ against $1/T$ for 3Y000G and $\ln[T^{1.55}\mathrm{d}(\Delta L/L_0)/\mathrm{d}T)]$ against $1/T$ for 3Y025G, 3Y050G, and 3Y077G. Each β_0 value was determined from the intercept of the plot using the determined Q value. Here, although both Q values of 3Y000G and 3Y025G have been already determined from the result in Fig. 7, their values were recalculated using the above plots whose accuracy is higher. The obtained results are shown in Fig. 9. Both Q values recalculated agreed nearly with those in Table 1. Each Q value of VD in 3Y025G, 3Y050G, and 3Y077G was smaller than that of GBD in 3Y000G, and in the range of 0.25–0.77 mass% GeO_2, the Q value of VD slightly increased with increasing GeO_2 content. The behavior of β_0 also showed the tendency similar to that of Q. According to Eq. 9, the sintering rate depends on both values of apparent activation energy (nQ) and apparent frequency factor (β_0^n). The nQ and β_0^n were, then, determined using the values of Q and β_0 in Fig. 9. As shown in Fig. 10, it was seen that both nQ and β_0^n increase with increasing GeO_2 content. It is, therefore, concluded that when the GeO_2 content increases, the sintering rate is enhanced because of the increases in the values of n with the GBD→VD change and of nQ and β_0^n of diffusion at the initial sintering stage.

Effect of GeO_2 addition

Based on the present results, the effect of GeO_2 addition on the initial sintering stage is considered as follows. Nakatani

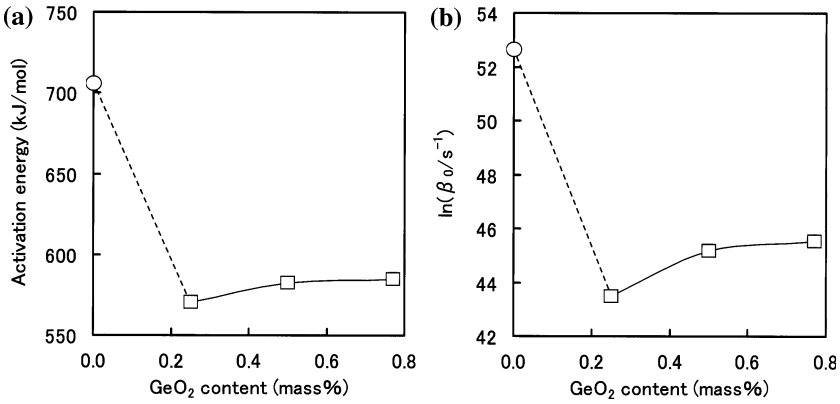

Fig. 9 Changes of activation energy and β_0 with GeO_2 content. (○) and (□) are GBD (n = 0.32) and VD (n = 0.45), respectively

et al. [14] have reported the microstructure in 1 mol% (0.8 mass%) GeO_2-doped 3 mol% Y-TZP sintered at 1,400 °C using high-resolution electron microscopy (HRTEM) and nanoprobe X-ray energy dispersive spectroscopy (EDS) techniques. In their analytical results, it has been showed that Ge^{4+} ions were observed in both grain interior and grain boundary, and segregated at the vicinity of the grain boundaries because Ge^{4+} ion content at grain boundaries was considerably greater than that in grain interiors. Taking into account this report, it is speculated that the increasing behavior of the sintering rate by GeO_2 addition directly relates to the solubility of GeO_2 in zirconia, and the sintering rate increases as the amount of dissolved GeO_2 increases. According to the result in Fig. 4, it is suggested that a part of added GeO_2 has already dissolved in zirconia particles at the temperature of ~1,050 °C. It is, therefore, concluded that as the result of segregated dissolution of GeO_2 in zirconia, the diffusion mechanism changes to VD and nQ increases with increasing GeO_2 content. According to the definition of β_0, the β_0 change in Fig. 9b corresponds to the surface energy of zirconia particles. This behavior of surface energy can be also interpreted by the segregated dissolution of GeO_2 on the zirconia surface.

As shown in Figs. 2 and 3, GeO_2 addition affects little the microstructure and grain growth at the hold-time condition of 2 h in the present sintering profiles. This is considered as follows. Matsui et al. [18] have reported the microstructure development in 3 mol% Y-TZP during sintering using HRTEM and nanoprobe EDS techniques. In this analysis result, it has been shown that no amorphous layer exists along the grain boundary faces in Y-TZP, but Y^{3+} ions segregate at grain boundaries over widths of ~10 nm. At 1,300 °C, the segregation of Y^{3+} ions appeared clearly and most of the grain boundaries in which Y^{3+} ions segregate transformed from tetragonal to cubic phases. When the sintering temperature attained 1,500 °C, the segregation of Y^{3+} ions grew sharply and the cubic-phase regions with high Y^{3+} ion concentration in grain interiors started to be formed from grain boundaries and the triple junctions in which Y^{3+} ions segregated. They named this diffusive transformation phenomenon *Grain Boundary Segregation-Induced Phase Transformation* (GBSIPT). Furthermore, Matsui et al. [19, 20] have also reported that the cubic-formation mechanism in 0.25 mass% Al_2O_3-doped 3 mol% Y-TZP during sintering is reasonably interpreted by GBSIPT model as with Y-TZP (without Al_2O_3 doping). Taking into account their reports, it is concluded that the cubic-formation behavior in 3Y000G–3Y077G during sintering proceeds by the GBSIPT mechanism, and at 1,500 °C, the cubic phase in them has been already formed in

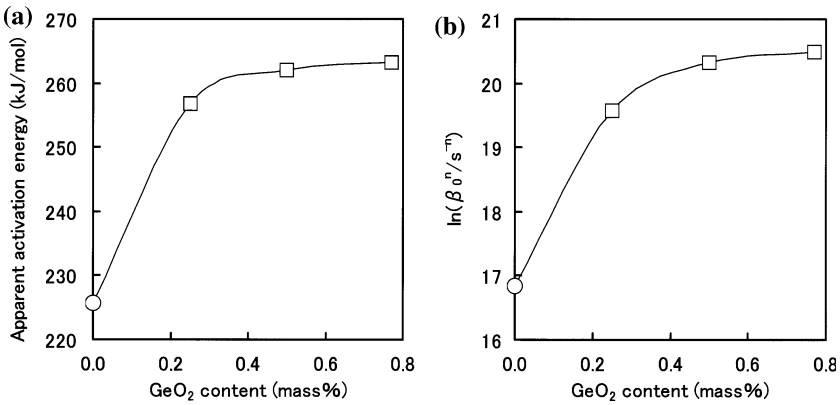

Fig. 10 Changes of apparent activation energy (nQ) and β_0^n with GeO_2 content. (○) and (□) are GBD (n = 0.32) and VD (n = 0.45), respectively

grain interiors as the tetragonal-cubic dual-phase grain structure.

According to the impurity-drag theory [21], when an impurity exists in a grain boundary, grain growth is depressed because the grain boundary migrates by dragging the impurity segregated in the grain boundary. Matsui et al. [18–20] reported that based on this theory, the grain-growth mechanism in Y-TZP is reasonably interpreted by the solute-drag effect of Y^{3+} ions segregating along grain boundaries. On the other hand, Yoshida et al. [13] have reported the small amount of dopant effect on the grain-growth behavior in Y-TZP. They experimentally revealed that the growth constant, which is related to the grain boundary diffusivity, increased as the ionic radius of dopant decreased and argued that the dopant cations segregated at grain boundaries change grain boundary diffusivity. Therefore, Ge^{4+} ions have the effect of enhancing GBD because the ionic radius of Ge^{4+} ions (0.067 nm) is smaller than that of Y^{3+} ions (0.104 nm) [22]. Taking into account these reports, it is supposed that at the conditions in the present sintering profile, the solute-drag effect of Y^{3+} ions rather than the effect of enhancing GBD of Ge^{4+} ions acts predominantly and as a result, the grain growths of 3Y000G–3Y077G show almost the same behavior.

Conclusion

In the present study, GeO_2, which is one of the additives, was noted, and the effect of GeO_2 addition on initial sintering of Y-TZP powder produced by the hydrolysis process was investigated. The following conclusions were obtained:

(1) The sintering rate in Y-TZP powder was remarkably accelerated by GeO_2 addition, and increased with increasing GeO_2 content. At the GeO_2 content of 0.77 mass%, the relative density attained 99% at 1,300 °C. The grain-growth process was not appreciably affected at the hold-time condition of 2 h in the present sintering profiles.

(2) The values of nQ and β_0^n of diffusion at initial sintering were estimated by applying the sintering-rate equation to the CRH data. The diffusion mechanism changed from GBD to VD by GeO_2 addition and both nQ and β_0^n of diffusion increased with increasing GeO_2 content. It is, therefore, concluded that when the GeO_2 content increases, the sintering rate is enhanced because of the increases in the values of n with the GBD→VD change and of nQ and β_0^n of diffusion at the initial sintering stage. This behavior can be explained by the segregated dissolution of GeO_2 on the zirconia surface.

References

1. Young WS, Cutler IB (1970) J Am Ceram Soc 53:659
2. Wang J, Raj R (1990) J Am Ceram Soc 73:1172
3. Wang J, Raj R (1991) J Am Ceram Soc 74:1959
4. Matsui K, Ohmichi N, Ohgai M, Enomoto N, Hojo J (2005) J Am Ceram Soc 88:3346
5. Matsui K, Tanaka K, Enomoto N, Hojo J (2006) J Ceram Soc Jpn 114:763
6. Johnson DL (1969) J Appl Phys 40:192
7. Moriyoshi Y, Komatsu W (1971) Yogyo-Kyokai-Shi 79:370
8. Johnson DL, Cutler IB (1963) J Am Ceram Soc 46:541
9. Johnson DL, Cutler IB (1963) J Am Ceram Soc 46:545
10. Moriyoshi Y, Komatsu W (1970) J Am Ceram Soc 53:671
11. Su H, Johnson DL (1996) J Am Ceram Soc 79:3211
12. Ikegami T (1998) J Ceram Soc Jpn 106:456
13. Yoshida H, Nagayama H, Sakuma T (2003) Mater Trans 44:935
14. Nakatani K, Nagayama H, Yoshida H, Yamamoto T, Sakuma T (2004) Mater Trans 45:2569
15. Kuwabara A, Nakano M, Yoshida H, Ikuhara Y, Sakuma T (2004) Acta Mater 52:5563
16. Yoshida H (2006) J Ceram Soc Jpn 114:155
17. Yamaguchi T (1984) Ceram Jpn 19:520
18. Matsui K, Ohmichi N, Ohgai M, Yoshida H, Ikuhara Y (2006) J Ceram Soc Jpn 114:230
19. Matsui K, Horikoshi H, Ohmichi N, Ohgai M, Yoshida H, Ikuhara Y (2003) J Am Ceram Soc 86:1401
20. Matsui K, Ohmichi N, Ohgai M, Yoshida H, Ikuhara Y (2006) J Mater Res 21:2278
21. Cahn JW (1962) Acta Metall 10:789
22. Shannon RD (1976) Acta Cryst A32:751